Computational and Structural Biotechnology Journal 18 (2020) 2799–2809

COMPUTATIONAL AND STRUCTURAL BIOTECHNOLOGY JOURNAL

journal homepage: www.elsevier.com/locate/csbj

The role of histone tails in nucleosome stability: An electrostatic perspective

Artemi Bendandi [a,b], Alessandro S. Patelli [c], Alberto Diaspro [a,b], Walter Rocchia [d,*]

[a] DIFILAB, Department of Physics, University of Genoa, Via Dodecaneso 33, 16149 Genoa, Italy
[b] CHT Erzelli, Nanoscopy, Istituto Italiano di Tecnologia, Via Enrico Melen 83, 16152 Genoa, Italy
[c] LCVMM, Institute of Mathematics, Swiss Federal Institute of Technology (EPFL), CH-1015 Lausanne, Switzerland
[d] Concept Lab, Istituto Italiano di Tecnologia, Via Enrico Melen 83, 16152 Genoa, Italy

ARTICLE INFO

Article history:
Received 20 July 2020
Received in revised form 23 September 2020
Accepted 24 September 2020
Available online 8 October 2020

Keywords:
Nucleosome
Electrostatics
Histone tails
Chromatin
Coarse graining

ABSTRACT

We propose a methodology for the study of protein-DNA electrostatic interactions and apply it to clarify the effect of histone tails in nucleosomes. This method can be used to correlate electrostatic interactions to structural and functional features of protein-DNA systems, and can be combined with coarse-grained representations. In particular, we focus on the electrostatic field and resulting forces acting on the DNA. We investigate the electrostatic origins of effects such as different stages in DNA unwrapping, nucleosome destabilization upon histone tail truncation, and the role of specific arginines and lysines undergoing Post-Translational Modifications. We find that the positioning of the histone tails can oppose the attractive pull of the histone core, locally deform the DNA, and tune DNA unwrapping. Small conformational variations in the often overlooked H2A C-terminal tails had significant electrostatic repercussions near the DNA entry and exit sites. The H2A N-terminal tail exerts attractive electrostatic forces towards the histone core in positions where Polymerase II halts its progress. We validate our results with comparisons to previous experimental and computational observations.

1. Introduction

In the nuclei of eukaryotic cells, DNA is compacted by wrapping around histone proteins, forming nucleosomes, the building blocks of chromatin. Nucleosomes consist of 147 DNA base pairs (bp) and a histone octamer core, formed by H2A, H2B, H3, and H4 histone protein dimers, and they are connected to each other by strands of linker DNA of varying length. The core domains of the histones are formed by three α-helices connected by short loops, mainly composed of positively charged residues [1]. Each histone has an intrinsically disordered N-terminal, and H2A histones possess an additional C-terminal domain [2], resulting in a total of ten "histone tails" per nucleosome, which contain approximately 30% of total histone mass. These domains bear a high concentration of positive charge and, along with counterions, help neutralize the high negative charge of the DNA backbone. The N-terminal histone tails are rich in glycine residues, the backbone carbonyls of which can form specific contacts with DNA phosphates. The flexibility of glycines facilitates changes in the local curvature of nucleosomal DNA [3–5]. Arginine residues are of particular interest, as stabilize the DNA around the nucleosome at 14 contact points [6]. Nucleosomes are by no means static entities, they participate in phenomena such as nucleosome sliding, a process in which DNA gradually repositions itself around histones, while maintaining contact with the histone core. [7,8] They also undergo partial or total disassembly [9,10], in order to tune transcription, DNA damage response, and gene expression [11–13].

Protein-DNA interactions are dominated by three types of phenomena: electrostatic interactions, hydrogen bonds, and hydrophobic forces. Direct electrostatic interactions, ionic interactions, and solvation are of particular importance in nucleosomes, because of the elevated charge of the interacting entities. [14] Solvation effects and electrostatic interactions are described by the Poisson–Boltzmann Equation (PBE), which uses a continuum mean-field description of the solvent, including dissociated salts, while solvated molecules are considered as continuous regions of lower dielectric value [15]. PBE theory has been used in both coarse-grained (CG) [16,17] and full atom approaches [18,19], using data acquired by solvers such as DelPhi [15] and APBS [20] or at a model-building level [21].

While Nucleosome Core Particles (NCPs) have been observed to be rather stable in dynamics, the histone tails present high

* Corresponding author.
E-mail address: walter.rocchia@iit.it (W. Rocchia).

https://doi.org/10.1016/j.csbj.2020.09.034

variability in their conformations, as expected of intrinsically disordered domains. Shaytan et al. [3] performed a 1 μs-long full atom Molecular Dynamics (MD) simulation, studying the dynamics of NCPs at varying ionic concentrations, observing, among else, that the majority of the contacts between the histones and the nucleosomal DNA are due to the histone tails, which rapidly adsorbed on the DNA surface during the simulation. The interactions and the number of contacts between histone tails and DNA strongly depend on their position with respect to the nucleosome dyad axis, and on the number of arginine, glycine and lysine residues. For example, the H3 N-terminal and H2A C-terminal tails form numerous contacts with the linker DNA and stabilize the DNA entry and exit regions of the NCP. Moreover, H3 tails have been observed in experiments [22] to form stable folded structures, possibly due to their high glycine residue content [23]. Histone tail interactions with nucleosomal DNA can locally alter the latter's geometry; in a 100 ns-long full-atom MD simulation of NCPs, it was seen that the largest fluctuation of the DNA groove width was caused by an arginine residue of the H2A N-terminal tail probing the DNA backbone [1].

The histone tails and their structural role have been studied in experimental works using a variety of methods, such as X-ray crystallography [24], Small Angle X-ray Scattering (SAXS), [25,26] Forster Energy Transfer FRET, [27] and Fluorescence Correlation Spectroscopy (FCS). Their mobile and intrinsically disordered nature makes studies using X-ray crystallography particularly challenging, [22,28,29] even though this method provides higher resolution data than fluorescence and scattering techniques, which do not allow for atomic level resolution. SAXS is often used in conjunction to other techniques, such as FRET and FCS to correlate different kinds of data. [30–32] However, structures in which the histone tails are completely lacking or badly resolved are often used.

Becker and Everaers, in their study of DNA nanomechanics, have developed a methodology to infer external forces and torques applied to a protein-DNA complex, in cases where the static shape of a structure is provided. [5] Using a bp-level CG representation of the DNA, they infer the values of the forces and torques acting on each individual bp. The amount of deformation that the DNA is subject to when in complex with proteins is deduced from comparison with free DNA segments, and free energy landscapes with respect to different degrees of freedom. The starting points were mean CG conformations of full-atom structures found in the Protein Data Bank. Their analysis allowed for the discrimination between force transmitting and non-transmitting protein-DNA contacts. However, the analysis conducted by Becker and Everaers is indirect, inferring the forces from the deformation of the DNA. Protein-DNA interactions are not explicitly taken into account. This methodology was subsequently applied to the nucleosome [33], including studies of features such as the twist defect, or the torsion of linker DNA connecting two adjacent NCPs.

The aim of this work is to provide information on the effect of the histone tails by studying the electrostatic interactions occurring in the NCP, and to propose a methodology to connect electrostatic calculations to the structural and functional features of protein-DNA systems. To that end, we connect observations made through the analysis of electrostatic calculations to structural features of the nucleosome. We infer the electrostatic forces acting on the phosphate groups of the DNA backbone by calculation of the electric field on the former. We study the electric field, electrostatic potential, axial and radial forces acting on each bp by performing PBE calculations on full atom structures extracted from the trajectory provided by Shaytan et al. [34] We analyze and compare our results on three sets of structures: structures in which the histone tails are included in the NCP, structures in which the histone tails have been truncated, allowing us to observe the electrostatic effects exclusively due to interactions with the histone core, and structures in which all charges except those of the histone tail residues have been put to zero, in order for the pure histone tail contributions to the electric field to emerge. We discuss the effect of the histone tails on the electrostatic potential in correspondence of DNA, along with a more general structural characterization of the NCP in terms of electrostatic interactions and DNA-histone contacts. We study the radial and axial components of the electrostatic force acting on the phosphates and their implications for the NCP structure. We conclude that the presence of the histone tails leads to non-trivial electrostatic effects of great significance for NCP stability, DNA unwrapping, and transcription.

2. Methods

2.1. Input structure selection and generation

The original PDB files and MD trajectory were taken from publicly available data, [34] from the work of Shaytan et al. [3] The structure (the "FN model" in [34]) is composed of the PDBPDBcode1KXode1KX5 crystal structure [35] and two 20 bp-long B-DNA segments of linker DNA. In order to identify the most stable histone tail conformations visited during the MD trajectory, we customized a clustering protocol, a variant of the well-established k-means algorithm, using the BiKi Life Sciences software. [36] Consistent with the fact that a linear combination of the atomic coordinates of two conformations does not normally correspond to a viable conformation, in this clustering algorithm no underlying vector space is assumed, and only the pairwise distance, i.e. the RMSD of the heavy atoms of the tails, was used. This has the further advantages that no reference structure is needed for the calculation and that the representative structure of each cluster, the medoid, is by construction a conformation observed during the MD. It is worth noting that the reliability of these structures in terms of being representative of equilibrium states depends on the overall exhaustiveness of the sampling performed in the trajectory. Shaytan et al. specify that their simulation explored conformational ensemble starting from a local quasi-equilibrium state.

We selected four medoids representing the largest clusters, in order to have the most diverse and representative structures in terms of the conformations assumed by the histone tails. The medoids are named medoid13, medoid15, medoid16, and medoid17, indicating the cluster that they represent. Cluster labels do not reflect the cardinality of the clusters. The number of structures in each cluster (population) and the percentage with respect to the total number of structures are provided in the Appendix (Fig. S2-S3).

We generated PQR files, i.e. PDB format files where atomic charge and radius replace beta-factor and occupancy, from the medoid PDB files via the PDB2PQR web server. [37] PQR files were used as input files for the DelPhi PB solver, which requires atomic radii and charges. We used the CHARMM force field setting for the PDB2PQR conversion, as it was the one used by Shaytan et al. in the MD simulations. After file conversion with PDB2PQR, we had to perform some manual changes to the DNA charge parameters due to nomenclature issues causing only partial recognition of the DNA structure. While the linker DNA was present in the original trajectory, and therefore in the medoids, it was truncated in order to conduct electrostatic analysis only on the NCP.

2.2. Electrostatic field and potential calculations

We calculated the values of the electrostatic potential and the electrostatic field on the positions of the phosphorous atoms belonging to the DNA backbone taking into account only protein

charges in three cases: intact structures, in which both the charges of the histone core residues and of the histone tail residues are taken into account, structures in which the histone tails have been truncated, and therefore only the charges of the histone core are taken into account, and structures in which only the charges of the histone tails are present. The charges of the DNA were switched to zero in all our calculations, so as to study the electrostatic contributions exclusively due to histones. We denote with SHL the Superhelical Locations on the DNA. Electrostatic energies were computed using the DelPhi PBE solver, interfaced with NanoShaper. [15,38] The solute was assigned a dielectric value of 2, and the solvent a value of 80. Salt concentration was set at 145 mM. Atomic partial charges and radii were taken from the PQR files. Other parameters assumed default values. The results obtained in this way are semi-quantitative. Indeed, the high charge on the NCP requires the adoption of the full non-linear PBE formalism and this would not, in principle, allow to calculate the effect due to one part of a system by just switching off the charges of the remainder. In order to assess the significance of this approximation, we followed the conceptual partitioning described in [15] and used the ionic potential at phosphorous sites in DNA as an estimate of the intensity of the entire non-linear effect, which also includes osmotic pressure and electrostatic stress terms. Ionic potential was calculated by subtracting the grid potential at the phosphorous' sites obtained with two PBE runs, one with physiological and the other with null ionic strength. According to the mentioned partitioning, in a fixed configuration the local electrostatic potential is the sum of the coulombic, reaction field (arising from the difference in polarizability between the protein and the solvent) and ionic contributions. As reported in the Supplementary Material, non-linear PBE calculations of the fully charged system show that the reaction field contribution is practically unaffected (absolute relative error $< 0.1\%$) by the introduction of the non-linearity and that the ionic potential amounts to the 2% of the former term, which, in turn, is of the same order of magnitude of the coulombic contribution generated by the histones' charges alone. This supports the correctness of the reported trends and patterns of electric field and potential and effects thereof.

2.3. DNA-Histone tail contact calculation

From the PDB files of each medoid we extracted the cartesian coordinates of all histone tail atoms and phosphorous atoms. The parsing of the PDB files was done using the class PDB of Biopython. [39] We generated DNA-Histone tail contact tables by selecting for each phosphorous atom the histone tail atoms within a cut-off distance in the range of 10 to 25Å. For each medoid we computed the total number of histone tail atoms that come into contact with each phosphate as a function of the cut-off distance. Using the CHARMM36 force field parameters we computed the electrostatic field generated by a phosphate and the neighboring histone tail atoms as function of the cut-off. In this work, we do not consider values of the cutoff higher than 25Å, because we observed that, after this threshold, the contribution of additional contacts with histone tail atoms to the electric field was not significant. The naming scheme of the chains present in the NCP and the residues belonging to each histone tail is summarized in Table 1. H-bond formation between each histone tail and the DNA in medoid13 were analyzed using the dedicated tool of VMD software.

2.4. Axial and radial electric field and force calculation

For each medoid we computed. the geometric center, and the covariance of the phosphorous cartesian coordinates. We then defined the axial direction as the eigenvector corresponding to the smallest eigenvalue of the covariance matrix, due to the shape of the system. The axial direction is computed once for the full medoid. First, we computed each phosphorous atom position with respect to the center and we projected the relative vectors on the axial direction. Finally, we converted the electric field [kT/Å/e] into the force acting on phosphates [kT/Å] by multiplying the DelPhi vector field by -e. In order to observe the trend of the spatial distribution in the electrostatic force, we considered the axial and radial components of the unitary vector corresponding to the electric field on each phosphate as reported by DelPhi. The resulting plots for the normalized and non-normalized radial and axial components of the electrostatic force are found in the Supplementary Material (Fig.S12-S23, Fig. S36-S71).

Table 1
Naming scheme used in this work for chains in medoids, and residues of each histone tail.

Molecule	Chain ID	Residues	Histone Tails (res. #)
Histone H3 (H3')	A (E)	1–135	N-terminal (1–44)
Histone H4 (H4')	B (F)	1–102	N-terminal (1–24)
Histone H2A (H2A')	C (G)	1–128	N-terminal (1–17) C-terminal (99–128)
Histone H2B (H2B')	D (H)	1–122	N-terminal (1–34)
DNA	I	−73–73	
DNA	J	−73–73	

3. Results and discussion

3.1. Structural characterization of medoids

The structures we selected to conduct our analysis of electrostatic interactions between histone tails and DNA are the representatives of the four largest clusters we obtained after performing a k-medoids clustering on a full-atom MD trajectory of the NCP. The details of this process are found in Methods. To quantify the difference between the histone tail conformations in each medoid, we used VMD to calculate the Root Mean Square Deviation (RMSD) of the residues belonging to the histone tails in each chain for all medoids, taking medoid13 (Fig. 1), representing the most populated cluster, as reference. The results of this comparison are seen in Table 2. The most diverse conformations are those assumed by the H3', the H2B, and the H2B' tails while the H2A' C-terminal tail presents similar conformations in medoids 15, 16, and 17. Medoids 15, 16, and 17 are depicted in the Supplementary Material (Fig. S1). Taking into account the electrostatic and mechanical effects that the plurality of interactions between the DNA and the histone tails produce, the use of structures obtained from the analysis of an MD trajectory emerges as almost a necessity. The use of the crystallographic structure in our analysis would overlook the adsorption of the histone tails on the DNA, their dynamics, and the changes they cause on the local curvature of the double helix. A variety of twist-defect nucleosome variants have been experimentally observed to exists in solution, [40] while only a few have been captured in crystal structures, such as 3AFA. [41]

In order to associate the conformational changes of the histone tails to electrostatic effects in NCPs, we calculated the number of histone tail atoms that come into contact with the phosphorous atoms in the DNA backbone, within a range of distances from 10 to 25Å. The resulting 2D plots are provided in the Supplementary Material (Fig. 8–11). We observed hot-spots of phosphate/histone tail interactions in the DNA entry and exit points, particularly at positive SHL. Numerous DNA-histone tail interactions in this region are known to be very important for DNA unwrapping, as we will discuss further in our analysis. Furthermore, there are regions of frequent DNA-histone interactions in chain J between bp 27 and 57, in which DNA interacts with both copies of H2A

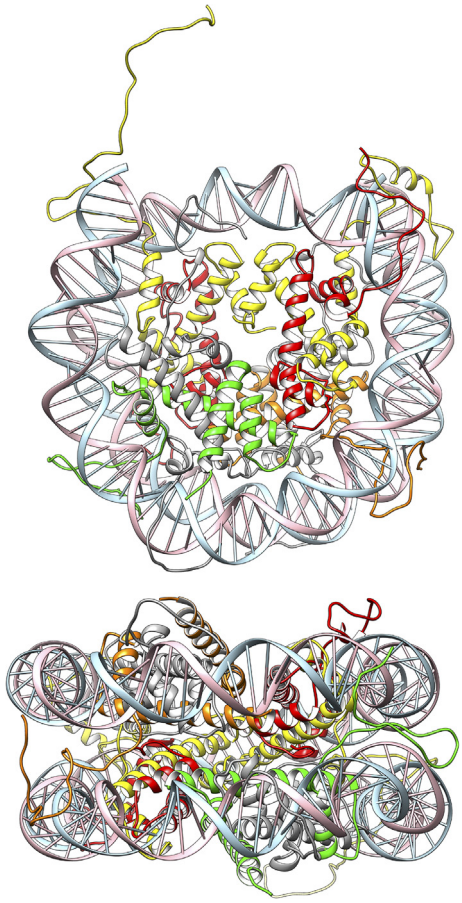

Fig. 1. Front and side view of the nucleosome. The histones and DNA are coloured by chain: histones H4/H4' in red, histones H3/H3' in yellow, histones H2A/H2A' in silver, and histone H2B in orange and H2B in green. (For interpretation of the references to colour in this figure legend, the reader is referred to the web version of this article.)

Table 2
Root Mean Square Deviation (RMSD) of histone tail residues among different medoids, compared to their positions in medoid 13. These values provide a quantitative indicator of the difference in histone tail conformations between medoids.

Histone Tail (res. #)	medoid15	medoid16	medoid17
H3 N-terminal (1–44)	7.743	8.816	4.885
H3' N-terminal (1–44)	11.014	18.034	13.593
H4 N-terminal (1–24)	5.163	6.576	6.038
H4' N-terminal (1–24)	8.728	8.266	12.033
H2A N-terminal (1–17)	5.089	6.555	4.548
H2A C-terminal (99–128)	3.556	5.517	2.376
H2A' N-terminal (1–17)	3.765	7.439	3.102
H2A' C-terminal (99–128)	4.833	4.437	4.489
H2B N-terminal (1–34)	5.489	9.022	18.974
H2B' N-terminal (1–34)	7.790	11.495	2.551

and H2B histones, as well as H4'. This is a key area for transcription, where Polymerase II has been observed to pause its progress. [42] We also observe marked differences in chain J between medoids 16 and 17: in the former, the histone tails are overall farther away, and are only closer to the DNA in the region of bp 33–35, where the DNA interacts with the H2B' tail. Overall, in medoid16 we have more localized tail-DNA interactions. Finally, in medoid17 we observe overall less contacts in negative SHL compared to other medoids.

The dynamics of the histone tails influence DNA geometry, causing, for example, DNA bulging in the entry/exit sites, and twist defects. In addition, histone tails form the majority of protein-DNA contacts in the NCP entry/exit sites. In terms of contacts, the histone tails make up 60% of all histone-DNA contacts. During the 1 μs simulation, up to 90% of histone tail amino acids formed direct or water-mediated contacts with the DNA, with no particular clustering of contacts toward the beginning or end of the tails. Arginine and lysine residues are found inserted in the DNA minor grooves, particularly the following residues: Arg8 and Arg26 of histone H3; Lys16 and Arg17 of histone H4; Arg11, Lys13 and Lys126 of histone H2A; and Arg29 and Arg30 of histone H2B. It is worth noting that, in the initial crystal structure, no interactions with the DNA were observed for the H3 and the H4 tails, and protein-DNA interactions through lysine residues were severely underestimated, indicating the pitfalls of only using a single structure in NCP analysis. In Shaytan et al., the histone tails exhibited large fluctuations, with an RMSD of more than 6Å, and were rearranged in the minor grooves, rapidly adsorbing on the DNA. The dynamics of the histone tails also depend on whether they adsorb on linker DNA or NCP DNA, the latter being much less flexible. The rapid adsorption of the histone tails on the nucleosomal DNA is also shown by the creation of H-bonds along the MD trajectory. The relevant plots are provided in the Supplementary Material (Fig. S80-S.89). The tail forming the most H-bonds is H3 (chain A), from initial 7 bonds stabilizing to a mean of 20 bonds. The smallest number of bonds was found in the N-terminal tail of H2A (chain C) and H3', which mostly interacts with linker DNA (less than 6 bonds). Finally, the tail of H2B (chain D) was already forming H-bonds with the DNA in the original structure, and their number oscillated around this value.

3.2. Electrostatic interactions

As a first marker of electrostatic interactions, we calculate the electrostatic potential (plots found in the Supplementary Material Fig. S4-S7) and the electric field exerted by the protein system on the phosphates, shown in Fig. 2. In the structures where the histone tails have been truncated ("no tails") the coulombic potential follows the periodicity of the DNA double helix: it is higher in the regions where the DNA backbone faces towards the histone core, and lower when it is facing away, presenting qualitative similarities to the trend of the forces described by Becker and Everaers. [33] The variations we observe in the "no tails" potential across medoids are attributable to the slight variations in DNA bp positioning along the MD trajectory, and to differences in core-DNA distances. The electric field follows the same trend. There is an obvious correlation between the vicinity of histone tail and phosphorous atoms and an increase in magnitude in the electric field (Fig. 2 "only tails field"). For example, we observe four regions of the DNA in which the electric field contribution of the histone tails is zero, indicating a lack of interaction with the histone tails in all four medoids: from bp −70 to −53, from −40 to −32 bp (in medoid16 the interactions on chain J are shifted away from the dyad by a couple of bp), bp 10 to 20 and 50 to 63. Conducting a proximity analysis between the phosphates of each DNA chain and the atoms of the histone tails, we see that in these regions there are very few (less than 100) or no atoms in a range up to 25Å.

3.2.1. DNA – histone tail interactions at the DNA entry/exit site

An area in which the contribution to the electric field owing to the histone tails is particularly marked can be consistently found between SHL −1.5 and −0.5, due to interactions with the tails of H3 and the C-terminal tail of H2A'. These tails appear to have approximately the same positioning across medoids, with the exception of medoid17, in which the H2A' C-terminal tail is inserted in the minor groove (Fig. 3D), a conformational change that is strikingly reflected on a more localized and higher in

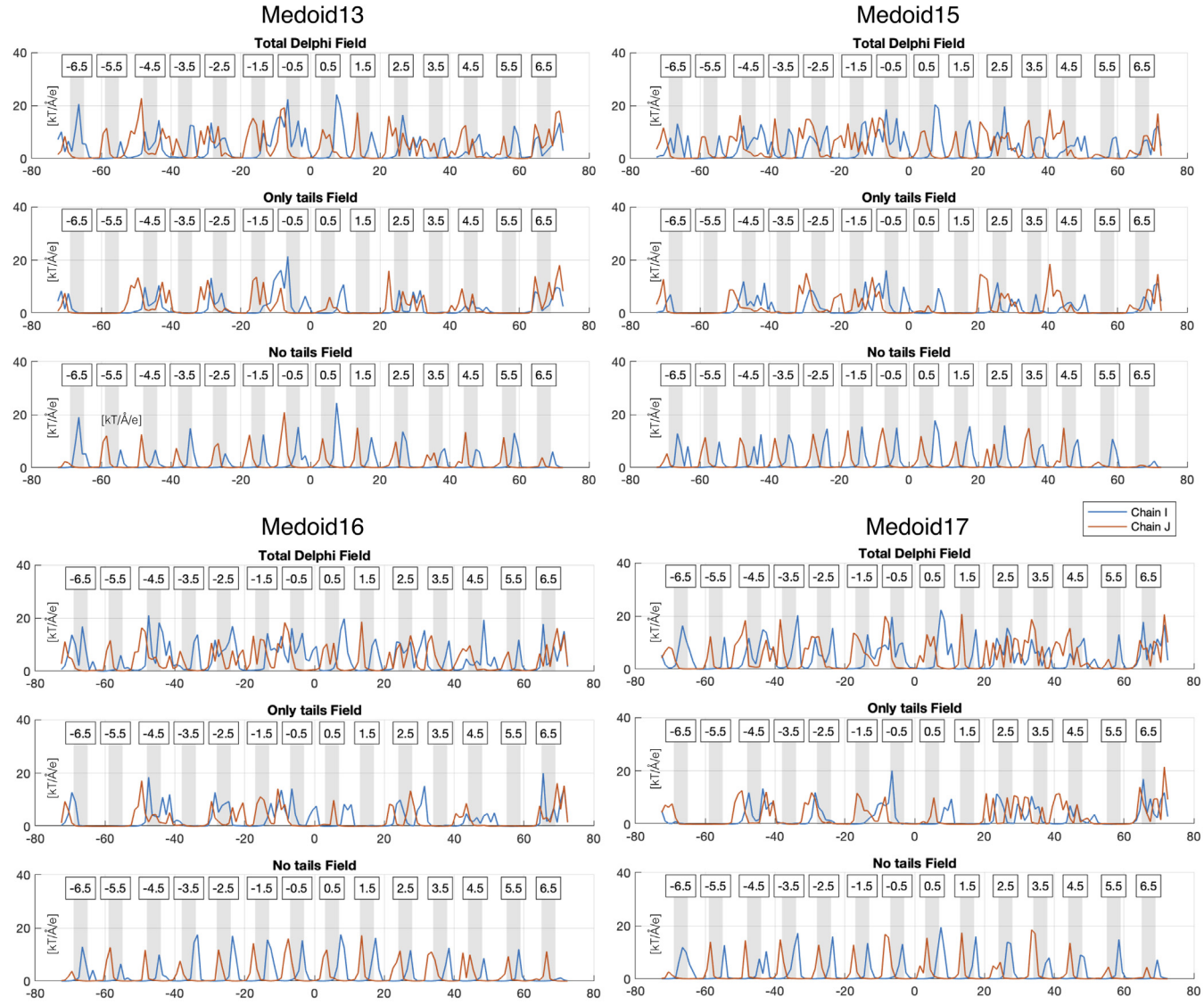

Fig. 2. Electrostatic field evaluated on the phosphates of the DNA backbone for DNA chain in each medoid. The calculations were performed on three versions of each medoid: the full structure, a version in which only the charges of the histone tails are non-zero, and a version in which the histone tails are truncated. The charges of the DNA have been put to zero in all structures, in order to consider only the electric field from DNA- histone interactions. SHL regions are highlighted in gray. In the "no tails" structures, the electric field clearly follows the periodicity of the DNA, while in the "only tails" structures the field shows a non-trivial dependence on the positions of the histone tails.

intensity peak in the electric field in SHL −0.5. Medoids 15 and 16 present more similar interactions in this area, compared to medoids 13 and 17. The electrostatic field in the former is characterized by a more diffuse signal, but lower in intensity compared to the more pronounced and localized peaks in the latter. We attribute this to the conformations of the H3' histone tail near the DNA backbone in medoids 13 and 17. Specifically, residues 27–39 of the H3' tail in medoid13 form a hairpin (Fig. 3A). The central residues in this configuration are two glycines, a threonine, and an alanine. On the other hand, in medoid17 this part of the H3' tail is mostly straight, giving rise to only one instead of two points of close contact with the DNA backbone near the DNA exit site, and overall larger distance between the tail and the DNA in the area between the two gyres. In medoid17 the hairpin is closer to the beginning of the tail, farther from the DNA. We see the repercussions of these two different conformations on the trend in the electric field in the DNA entry site as well (bps ± 73). Here, medoids 13 and 17 present more moderate electric field values, as less close contact points exist between the tail and the DNA backbone. Finally, in medoids 16 and 15 the "hairpin" involves less residues than in medoid13 (6–7 residues).

The C-terminal tail is fundamental to the changes in the electrostatic interactions, as the conformation of the H3' tail between the two gyres is mostly conserved, while the C-terminal tail's conformation varies greatly. Since the H3' tail is known to interact more with linker DNA than with nucleosomal DNA [3], this behavior is consistent with expectations. There is a peak on the dyad in medoid13 and medoid15, which is lacking in medoid17. This is due to a shift of the last two residues of the C-terminal towards the dyad, in a position where the DNA double helix is at its closest to the core. In medoid16, this peak is shifted by a couple of bps but it can be ascribed to the same interaction.

Finally, interesting DNA-histone tail interactions occur at the DNA exit site (bp 63–73). These two superhelical turns are embraced between the short H2A' C-terminal tail from the interior and the long H3 tail, which protrudes between the two DNA gyres, from the exterior. The most diversity is seen in medoids 15 and 17, attributable to very different H3 tail conformations. The end of this

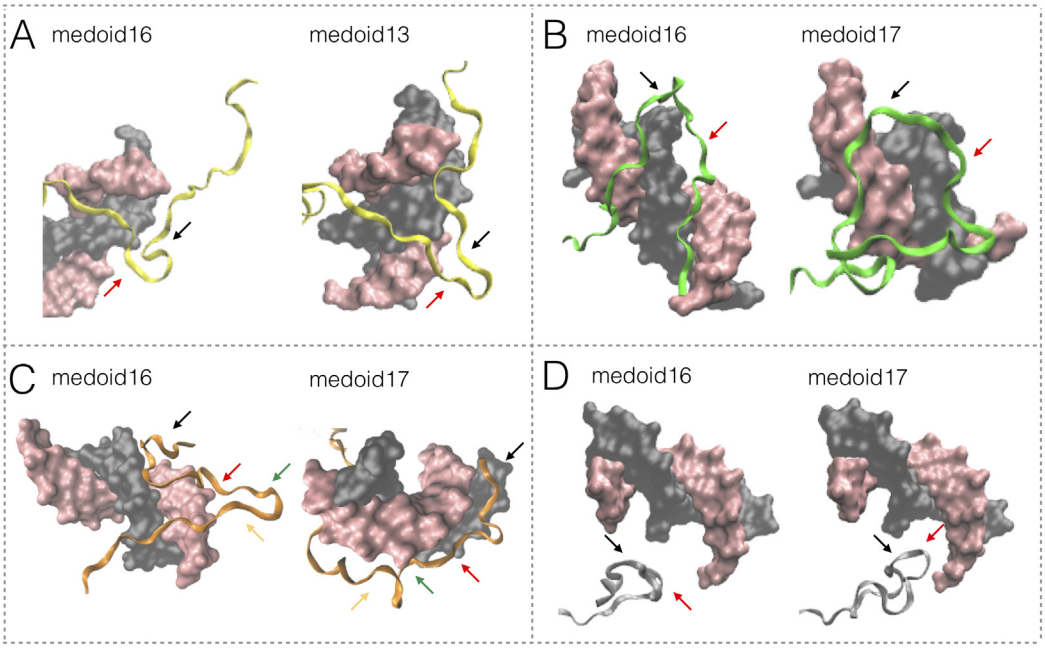

Fig. 3. A: Conformations of the H3' histone tail near the DNA backbone in medoids 16 (left) and 13 (right). Residues 27–39 of the H3' tail in medoid13 form a hairpin. In medoid16 this part of the H3' tail is mostly straight. In medoids 15 and 17 a similar hairpin (not shown) is present but it involves less residues. B: All medoids present a peak in the electrostatic field at bp −30 (chain I), because of interactions of the H2B' tail with both DNA gyres. In medoid16 (left), the H2B' tail is positioned farther from the DNA than, for example, in medoid17 (right). C: In medoid16 (left) the H2B tail is inserted into the minor groove, between bps 49 and 53, while in medoid17 (right) it assumes a circular conformation on the DNA. D: The insertion of the H2A' C-terminal tail in the minor groove in medoid 17 (right) versus a larger distance from the DNA in other medoids (medoid16 pictured in the left) causes a more localized and intense peak in the electric field in SHL −0.5.

tail exercises repulsive forces on bps −7 – −10 on chain I, on the other DNA gyre. The shift in the force once again reflects the different conformations of the H3 tail. Observing the 3D structures, we notice that a portion of the H2A' tail forms a short α-helix composed by three residues: Ser113, Val114, and Leu115. The final residues of the H2A' C-terminal tail are essentially in the same position in both medoids. Chain I of the DNA mainly interacts with the H2A' C-terminal tail, while chain J with the H3 tail. The ability of electrostatics to capture slight structural variations is shown by a peak in bp 66 in chain I, present in medoids 16 and 17 but absent in medoids 13 and 15, correlated to a slightly different conformation of the C-terminal tail.

3.2.2. Histone tail effect at negative and positive SHL

We see that all medoids present a peak in the electrostatic field in bp −30 (chain I), because of interactions of the H2B' tail with both DNA gyres. In medoid16, this interaction is displaced with respect to the other medoids: the H2B' tail forms a double hairpin, and is positioned slightly farther from the DNA than, for example, in medoid17 (Fig. 3B). Variations of this double hairpin are also found in medoids 13 and 15. The first residues of the H2B' tail are closer to the DNA backbone than the loop of the hairpin. This region is also interesting because the H2B' tail protrudes from between the two DNA gyres, exerting axial and radial forces on the DNA. In conjunction with the presence of the H4 tail in the vicinity, and observing the atomistic structures, we see that the two DNA gyres are closer together. The same effect can be seen in other regions of the NCP where the histone tails protrude between the two gyres, especially in the DNA entry and exit sites and the region around bp 50 (chain I). Between SHL −1.5 and −2.5 we observe only minor electrostatic interactions in medoids 13 and 17. This is not the case for medoids 15 and 16, which present peaks of moderate intensity in those positions on chain J, a behavior which is once again reflected on the contacts in our proximity analysis by an increase in the number of histone tail atoms within the cutoff. There is a larger number of interactions with the H2B' tail at a 10Åthreshold in the medoid17, while in the medoid13 they are shifted at distances of 14 and 18Å.

There are various interactions between the DNA and the N-terminal tails of histones H3 and H4. This part of the DNA is embraced between these two tails, as the H3 tail emerges between the two gyres. Indeed, the variations that we observe in the electrostatic field on the phosphates of the J chain are due to interactions with the H3 and H4 tails in SHL 0.5 (corresponding to −0.5 on chain I). The area between bp 20 to 32 presents a lot of electrostatic features in all medoids, owing to interactions of the DNA backbone with the tail of H4. Only medoid17 presents significant conformational variability with respect to the others: in this case, the tail appears to be shifted in parallel towards the external part of the DNA gyre, a conformational change reflected in a shift in the respective electric field peaks, and on variable axial forces acting on the DNA. In our proximity analysis, we see more diffuse interactions in the region between bp 20 and 40 in medoid17, compared to much more localized interactions in the same region of medoid16. This conformational change has repercussions on the forces acting on the DNA backbone.

The region that expresses the greatest heterogeneity across different medoids is from bp 20 to bp 53, where the N-terminal tails of histones H2A', H2B, and H4' interact in succession with the DNA. In the region from bps 47 to 53, the tail of H2B protrudes between the two DNA gyres. We still observe some similarities among medoids. The most striking example is that of bps 32 to 40, in which the electric field on the phosphates is almost null in medoids 13 and 16. This is caused by the increasing distance of the H2B tail from the DNA, after it emerges between the two gyres. Once again, we observe an overall lack of contacts between DNA and protein atoms, while in chain I of medoid17 there are at least 100 atoms of the histone tails in the range from 10 to 25Å. Medoids

16 and 17 are also characterized by an overly low electrostatic signal between bps 40 and 53, owing to the great conformational heterogeneity of the H2B tail. In medoid17 the first residues of this chain fit closely into the minor groove, between bps 49 and 53, in a completely different conformation compared to medoid16; a hairpin in the latter, a circular conformation in the former (Fig. 3C).

3.3. Radial and axial electrostatic forces on the DNA

It must be noted that the present force calculations are based on representative structures extracted from a MD trajectory where DNA unzipping has not been observed and therefore they could lack some characteristics that are precursory of this process. The plots of the radial and axial electrostatic forces we refer to in the text are provided in the Supplementary Material (Fig. S12-S71), for reasons of space. In the "no tails" structures, there is a periodicity in the trend of the force roughly corresponding to the double helix pattern, overwhelmingly attractive towards the core. The force is particularly attractive at 14 points, which correspond to the 14 contact points where the nucleosomal DNA is in proximity of arginines on the histone core. The histone core and histone tails cause contrasting effects on the DNA backbone, resulting in opposing forces. By examining the plots of the total radial force we see that the repulsive forces are mostly due to interactions with the histone tails, while the radial force is attractive in regions with a low or very low number of DNA/histone tail contacts. We observe sometimes opposed forces acting on the phosphates of pairing bases, which may have mechanical repercussions on the double helix. A characteristic example is the SHL 2.5 region on medoid13. The N-terminal tails of H3 and H2B protrude between the two DNA gyres, stabilizing the latter's superhelical structure in the NCP. These interactions are particularly strong near the dyad axis, and in two more regions approximately ±50bp from the dyad, where the H2B tails interact with the DNA. [43] Indeed, by looking at the contributions of the histone tails to the radial and axial components of the electrostatic force we see that on the dyad, on ±50bp and around that position the forces are attractive.

In order to have an insight on the dominant effect of the axial component of the electrostatic force on the phosphates, we examined their distribution on the different structures (histograms shown in Supplementary Material Fig. S24-S35). In the absence of histone tails, the axial forces produce a stabilizing effect. In the "no tails" version of medoid16 the forces on the lower DNA gyre present a wider distribution. The effect of the histone tails is markedly attractive/repulsive, with the exception of medoid17, where it is evenly distributed along the lower gyre, but follows the same trend. For the total axial force on medoid17 there is no clear trend in the lower gyre, and the forces are uniformly distributed in the upper gyre as well. The lack of a dominating overall effect implies a less stable structure in which the two DNA gyres are not kept together as steadily as in other medoids. Similarly, in medoid13 the axial forces are evenly distributed, even though slightly attractive and slightly repulsive trends are observed on the upper and lower gyre respectively.

3.3.1. The effect of histone tails on DNA unwrapping

The forces that the histone tails exert on DNA can be studied in conjunction with the positions in which DNA is known to detach from the histone core, or attach more strongly to it. For example, the first barrier encountered during transcription by Polymerase II is at approximately 40 bp from the dyad. [42] There are strong attractive radial forces immediately after bp ±40 on both DNA chains, even in cases in which the forces were repulsive immediately before that position. This behavior could be attributed to the nearby arginine residues of the tails of both copies of H2A. The electrostatic interactions on neighboring phosphates are similar across medoids, with two exceptions: slightly lower intensity of the electric field in medoid13, owing to a larger distance between DNA and protein atoms, and a spike in medoid16, where Lys28 of the H2A tail is found closer to the DNA I chain near bp −47. The interactions with the J chain of the DNA present more heterogeneity, but there are similarities between medoids 13 and 17 and medoids 15 and 16: in the region from bp −40 to −45, the former present more intense the electric fields, while the latter present lower values. Once again, this is directly linked to the different positioning of the H2A' N-terminal.

An important feature that transpires from the total radial components is that the histone tails are responsible for a repulsive radial force of varying intensity across medoids. This force is present when the histone tails protrude from between the two DNA gyres in the DNA entry and exit regions, favoring a possible unwrapping process. In Kono et al. it is stated that the outer turn of the DNA in NCPs unwraps following a three-step asymmetric procedure. [44] First, 5bps unwrap from one end of the DNA, followed by 5 more bps from the same end, without further increase in free energy. Then, unwrapping starts at the other end, where a total of 10bps is unwrapped in the same way. The process is completed by the unwrapping of 15 more bps at both ends. NCPs have also been experimentally shown to unwrap in stages [45], with the first half of the bps unwrapping at a low force, while the second half requires a higher force. The H3 tail remains in contact with the DNA near the entry and exit points of the NCP until the initial 10 bp are peeled off both sides. During the following stages, gradual changes are observed in the contacts between the DNA and the H2A/B tails. The positions on the NCP in which unwrapping is seen to be temporarily halted in Kono et al. are correlated with the positions of the histone tails. In particular, the first five bp on J chain on the entry sites of our medoids are in contact with histone tails H2A C-terminal and H3, while bps on chain I present contacts in the first 8 bps with these tails. Interestingly, in the SHL ±3.5 region, which corresponds to the end of the total 25 bp that unwrap from each side, there is a relative absence of DNA-histone tail interactions, indicated also by a lack of a significant electrostatic field influence due to the histone tails in that region. The total radial force is attractive here, due to the dominant effect of the histone core, but it is zero or even repulsive in the regions immediately before this. We conclude that the histone tails can tune DNA unwrapping, by increasing the tendency of the DNA to unwrap from the histone core.

3.3.2. Repercussions of histone tail truncation

The truncation of the H3 and H4 tails has been shown to produce opposite effects [25]: the removal of the arginine- and lysine-rich H3 N-terminal favors DNA dissociation from the histone core, while H4 truncation stabilizes the wrapped conformation. The radial forces exerted by the histone tails tell a different story: in this region the force is repulsive in all medoids except for chain J in medoid 17, highlighting the role of Lys36. The total axial components are mostly repulsive on both chains in the DNA exit site, indicating that it tends to move upwards from the dyad plane, but they are mostly attractive in the entry site. The end stretches of the DNA spontaneously unwrap 1–10% of the time (the propensity to unwrap is sequence dependent), and target sites located inside the NCP (at smaller SHL absolute value) are less accessible than sites located near the DNA entry-exit points [46]. In Iwasaki et al., four mutant nucleosome structures were studied, each of which lacked histone tails from a specific histone. [43] H2B and H3 deletion substantially decreased NCP stability, while H2A and H4 deletion caused opposite effects. H3 deletion was seen to enhance unwrapping at the DNA entry and exit sites of the NCP, very near the points where the H3 tail protrudes from the core (Fig. 4D), possibly enhancing nucleosome sliding. In our analysis,

we see repulsive axial forces with respect to the NCP core near bp 10 of chain I, a region of the DNA in close interaction with the glycine- and lysine-rich - therefore flexible and positively charged - H4' histone tail.

In the structures where the histone tails were truncated, all medoids present a repulsive trend in the axial component in chain J from bp 0 to −19, with a minimum on bp −7. In the same area chain I presents the same jigsaw pattern we encountered in the electric field and electrostatic potential, while there is an absolute maximum in the force acting on bp 7. In the total axial force, we see a switch from an attractive trend in medoids 13 and 17, where less atoms are found near the DNA backbone around bp 35, to a repulsive trend in medoids 15 and 16, in which there are more atoms in that region. In chain I there are overall repulsive forces in all medoids from bp 1 to bp 18, with a peak on bp 7, which we attribute to the histone core, and particularly the loop connecting the α-helices of histone H4'. Furthermore, there is a region presenting variability across medoids from bp −40 to −55. As we mentioned in our analysis of the electric field, this region presents interactions with the H2A N-terminal tail, and the contribution is due to the histone tails, as we see from the non-normalized forces. We attribute to the action of the H2A N-terminal tail, that embraces the DNA gyre from above. Comparing the total axial components to the "only tails" structures there is a repulsive force in SHL −5.5 across medoids due to the core, while a contribution from the tails is absent. As in the case of radial forces, sometimes the core and tails cause contrasting effects. For example, in SHL 5.5 chain J the tails present a consistently repulsive trend, while the total contribution is attractive.

Brower-Toland et al. [45] observed that the removal of the H2A and H2B N-terminal tails induced a decrease in the histone-DNA interaction strength at a position ±36 bp from the dyad axis. In our medoids, the H2A and H2B N-terminal tails protrude from between the two DNA gyres in positions near bp ±30 (Fig. 4A). Comparing the total electric field on and near those DNA bps with the contributions of the histone core and histone tails, we see that the electric field is mainly due to the histone tails in those points. In order to see if these tails are a stabilizing or destabilizing component of the NCP, we examine the effect of the histone tails on the axial component of the force. In those positions the histone tails have a stabilizing effect, as the axial forces present an overall attractive tendency. Juxtaposing the axial force contribution of the histone core and that of the histone tails in that position, we see that the latter is of higher intensity. However, the radial component shows that the histone core exercises a strong attractive force, while the histone tail contribution is either close to null for bp-30 or even repulsive for bp30.

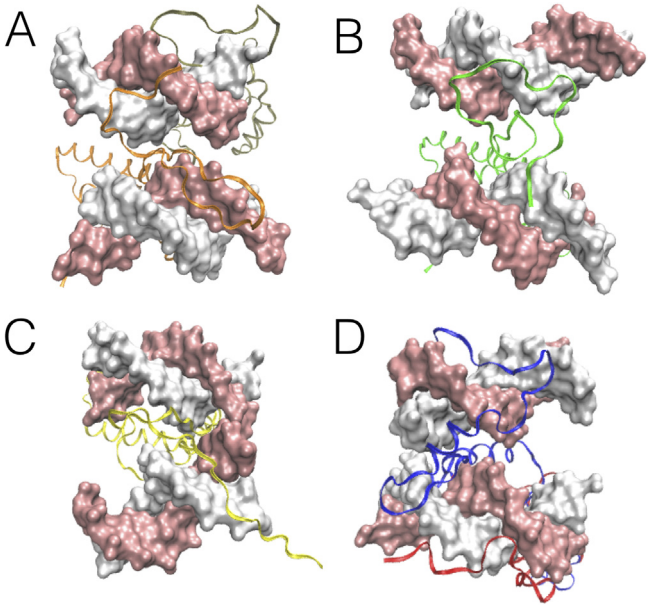

Fig. 4. Histone tails protruding from between the two DNA gyres of an NCP. Medoid13 was used as reference. A: H2A (in gray) and H2B (in orange) N-terminal tails. B: H2B'. C: H3' (NCP DNA exit site). D: H3 (in blue) and H4 (in red) embracing the DNA in the NCP entry site. In the sites where histone tails protrude from between the two DNA gyres, the latter are brought closer together, stabilizing the structure.

In most approaches, the role of the C-terminal tail appears to be downplayed. It is interesting to see how the truncation of the H2A C-terminal domains change nucleosome dynamics, as they have been observed to increase the nucleosome sliding rate [47]. Cells expressing truncated H2A C-terminals showed increased stress sensitivity and nucleosome mobility. This tail has two important functions: it stabilizes the NCP and mediates interactions with other proteins. Simultaneous deletion of histone tails from more than one histone has been observed to relate to compromised cell survival in yeast [48]. In our analysis, we see the important effects that the C-terminal tail has on nucleosome electrostatics, since even a shift of two residues can produce significant electrostatic effects.

Besides histone tail truncation, sometimes entire histones can be missing from the NCP, [49] forming Partially Assembled Nucleosome States (PANS). Nucleosomes have the ability to dissociate entirely in histones and DNA, and then reassemble [50], in a process driven by electrostatic interactions. Rychov et al. [9] analysed PANS with MD simulations. The nucleosome formation procedure was seen to occur as such: the two H3 and H4 dimers bind to the DNA, forming a tetrasome, followed by the sequential addition of H2A and H2B dimers. MD studies on PANS reveal that the nucleosomal DNA is drastically deformed when histones H2A or H2B are missing, but the loss of H3/H4 does not have the same impact on DNA conformations, because of the action of the H2A C-terminal tail, which fills the space left empty by missing histones. The method we propose in this work can be applied on structures representing intermediate states of association/dissociation MD trajectories, to investigate the fleeting contacts formed between the histone tails and the DNA, and the role of the histone tails in NCP assembly.

3.4. Arginines and Lysines: key histone tail residues

The particular importance of arginines and lysines is evident from several interactions in NCPs. Their positions in the nucleosome are illustrated in Fig. 5. For example, looking at bp −20 of chain J in medoids 16 and 17 we see a change in the trend of the force from attractive to repulsive, attributed to a variation in interactions with two particular arginine residues: Arg17 and Arg19 the H4'. In medoid 16 these arginines are found at a distance of 3Å and 12Å respectively from the phosphate of bp −20. However, in medoid 17 their respective distances from the same phosphate are 8Åand 6Å. In medoid13, on chain J bp 54 there is a strong repulsive force, because of close interactions of the phosphate with Lys17 of chain D (H2B). In medoid16 there is a repulsive force on bp −65 of chain I, found close to chain E Arg52, and on bp −54 on chain I, close to chain D Ser52/53. Interestingly, there is no effect on the corresponding bps in chain J in either case. In medoid15, on the other hand, there are strong repulsive forces on bps belonging to chain J, notably on bp ± 65, because of a contact with chain E Lys56. In this case we notice no corresponding effect on chain I bps.

The conformations and dynamics of the histone tails are greatly altered by Post-Translational Modifications (PTMs), sometimes

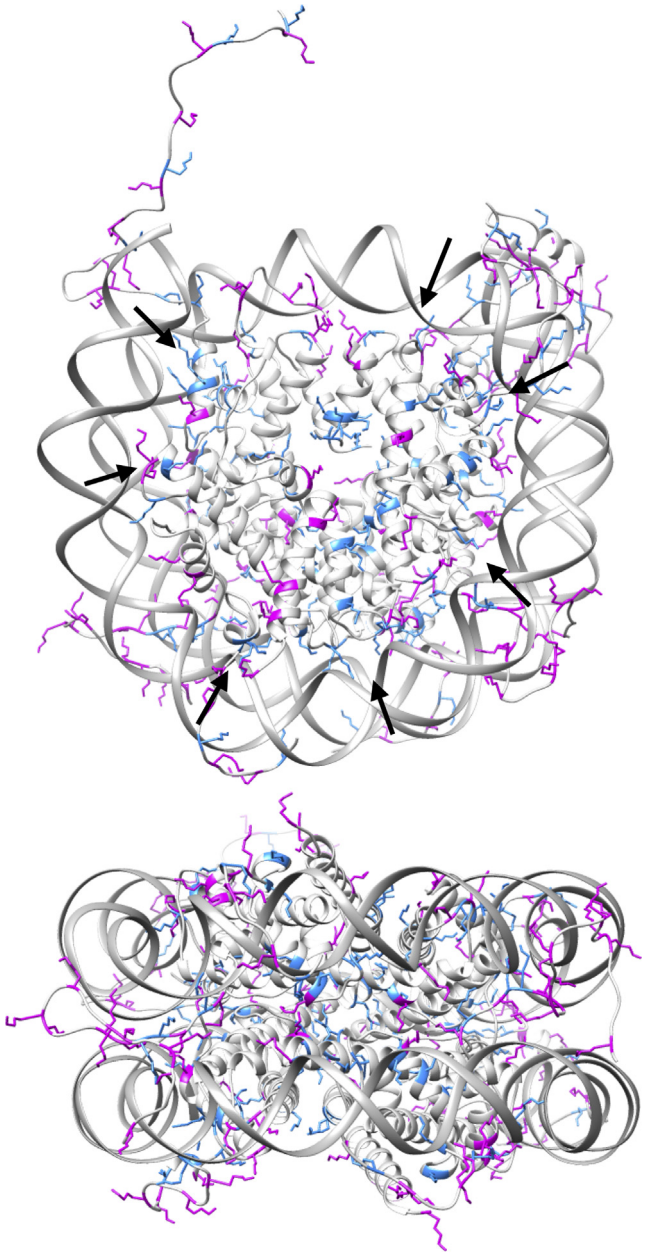

Fig. 5. Arginine (in blue) and lysine (in magenta) residues in the nucleosome. The presence and location of these residues strongly affects nucleosome electrostatics. The DNA is anchored to the histone core in 14 contact points with arginines, 7 on each side of the NCP, indicated by arrows. Lysines and their PTMs, especially acetylation, impact on inter- and intra-nucleosome interactions.

triggering effects that can supersede native electrostatic interactions. Acetylation leads to a reduction of the overall positive charge, reducing self-repulsion, and facilitates more hydrophobic interactions. Furthermore, it increases the volume occupied by the side chains of the affected residues, with steric implications, and drastically reduces the interactions of the H4 tail with the acidic patch of the same or neighboring NCPs, influencing tail-bridging and inter-NCP interactions. Hyperacetylation of the H4 histone tail [51] can result in enhanced DNA accessibility to DNA-binding proteins, [52,53] acting as a chemical signaling method for transcription. Acetylation of H4 tails increases their propensity in forming α-helices, ultimately making them shorter, [25] further hindering their interactions with acidic patches. The H4 tail forms the largest number of protein-DNA contacts at physiological salt concentration, particularly in the region between residues Lys16 to Arg23. [23] These contacts are disrupted upon the presence of PTMs. Both H3 and H4 acetylation enhance DNA unwrapping in ionic concentrations higher than physiological. Moreover, H3 acetylation renders the NCP more sensitive to counterion-induced dissociation and histone dimer exchange between NCPs, while H4 acetylation has opposing consequences. [10] H3 acetylation enhances DNA breathing at physiological ionic concentrations, while H4 acetylation has this effect at higher ionic concentrations. At low concentrations, acetylation was not observed to correlate with DNA binding propensity. Potoyan and Papoian [51] observed that Lys16 acetylation disrupted H4 tail binding and folding landscapes, enhancing α-helix formation. The same PTM was seen in FRET experiments to result in a tightening of the linker DNA in the NCP entry and exit points, opposing the tail-bridging effect and weakening inter-NCP interactions, therefore disrupting NCP stacking in the chromatin fiber. Progressive acetylation of the H4 tail showed cumulative effects, [27] caused by progressive charge reduction and increased hydrophobicity induced by the clustering of acetyl groups.

Tail truncation and lysine hyperacetylation produce similar results, from the electrostatic point of view, since the positive electric charge is reduced in both cases. For example, H3 and H4 tail truncation has also been observed to increase DNA accessibility, as is the case with hyperacetylation of these tails. [54] The steric implications of these two processes are naturally different, and result in different configurations and interactions between residues in the NCP. PTMs are often hard to study because they are challenging to detect reliably in a sample containing many nucleosomes. However, by understanding the electrostatic implications of the charges present on the histone tails and by examining the electrostatic interactions that take place in their absence, we can improve our knowledge on the consequences of PTMs.Table 3.

3.5. Extension to CG models

Becker and Everaers, [33] in their work on the CG base-pair level model of the nucleosomal DNA used X-ray structures to infer the forces acting on the DNA. They observed a periodic pattern of high force peaks, corresponding to the contact points of the nucleosomal DNA and the histone core. These correspond to peaks in the elastic energy of the DNA, and the pattern is similar to the trend we observe for the electric field and the axial component of the force in structures in which the histone tails are absent. Furthermore, Becker and Everaers analyzed the deformations of the nucleosomal DNA, and extrapolated the forces and torques that would be necessary to induce such deformations, interpreting them as interactions between the nucleosomal DNA and the histone tails. However, a single static structure was used, and therefore the large variety of different histone-tail we observed in our analysis was not taken into account. In our simulations, the electrostatic potential and electric field presented this periodicity in the structures that do not include the histone tails. In addition, we clearly observe peaks in the intensity of the radial component of the electrostatic force on the 14 contact points. Our results clearly indicate that the histone tails are of central importance to the electrostatics of NCPs, and that forces caused by these interactions have important repercussions in the stability of the NCP, in DNA unwrapping, and therefore in transcription. We observe a non-trivial dependence between the presence of histone tails, their distance from the DNA, and the magnitude of the electric field.

Studies elucidating the separate effects of histone core and histone tails, and the sensitivity to the conformational changes of the latter, can prove very useful to construct improved CG models and to help explain phenomena that might otherwise be puzzling. The forces acting on each phosphate group, which are mainly of

Table 3
Summary of properties of histone tails observed in this work: Histone tail Role in the dynamics of the nucleosome, and particular electrostatic and conformational features of different medoids.

Histone Tail	Properties	Medoid Features
H3/H3'N	Interacts with linker DNA	Repulsive radial forces in all medoids (Lys36)
	Can form stable folds	(H3') straight in medoid13, hairpin in others
	Truncation hinders NCP stability	
H4/H4' N	Truncation favors NCP stability	Diffuse interactions in medoid17, localised interactions in others
	Interacts with acidic patch	Large number of contacts with DNA in SHL −0.5 in all medoids
H2A/H2A' N	Halts PolII	Intense electric field in medoids 13 and 17
		(H2A) Lys28 very close to DNA causes spike in medoid16
H2A/H2A' C	Embraces DNA	Interaction on dyad (H2A') in minor groove in medoid13,
	Interacts with linker DNA	off dyad in medoids15/16, No interaction in medoid17
	Stabilizes PANS	Field peak on bp 66 in medoids 16/17
H2B/H2B' N	Protrudes between DNA gyres	(H2B) circular conformation in medoid 16, hairpin in medoid17
	Truncation hinders NCP stability	(H2B') double hairpin in medoid16
	Great conformational heterogeneity	(H2B) inserted in minor groove in medoid17

electrostatic origin and have been derived from DelPhi calculations, can be used in combination with the sequence–dependent cgDNA+ [55] model, which includes the mechanical forces acting on the DNA backbone and explicitly treats each base and each phosphate group. It is possible to minimize the CG energy predicted by cgDNA + with external constraining forces applied to each phosphate group. This approach would allow the exploration of the CG energy landscape as a function of the DNA sequence with given fixed forces separating them in those caused by the histone core ("no tails" structure), and by the histone tails ("only tails" structure). We believe that the effects of the histone tails should be a central part of CG models regarding nucleosomes and chromatin. Furthermore, studies that infer the forces acted upon DNA by the histone tails and connect them to the structural features of the nucleosome can be particularly useful, since histone tails are notoriously hard to observe experimentally at atom-level, or even residue-level, resolution. Finally, electrostatic forces are a fundamental ingredient in CG models of such highly charged systems and can provide a mechanistic interpretation of chromatin dynamical processes and conformational equilibria.

4. Conclusions

In this work, we propose a methodology for the study of protein-DNA electrostatic interactions and we apply it to clarify the effect of the histone tails on the NCP. Our methodology correlates electrostatic interactions and spatial conformation at the residue level with mechanical effects and repercussions on their structure and function. Studying the NCP, a complex protein-DNA system, we were able to identify the possible electrostatic origins of many effects, such as spontaneous DNA unwrapping, NCP destabilization upon histone tail truncation, and the key role of specific arginine and lysine residues. We study four representative structures extracted from a 1 μs full-atom MD simulation in explicit solvent, to capture some relevant conformations of the histone tails, and we separate their electrostatic contributions from those of the histone core, to assess their individual importance. We construct contact maps of the histone tails with the DNA, to study the correlation between the number of histone tail atoms in proximity to the DNA, and the intensity of the electrostatic interaction. We stress the role of H2A C-terminal tail: small changes in the positioning of this short tail had a significant impact on the electric field, implying that this often overlooked feature of the NCP holds particular importance in the dynamics of the nucleosome. We consistently observed that, in the places where histone tails protrude from between the two DNA gyres, the latter appear "pinched" closer together (Fig. 4), and perceive a repulsive radial force, pushing them away from the histone core. Notably, the H2A N-terminal tail exerts attractive electrostatic forces towards the histone core in positions where Polymerase II is known to briefly halt its progress along the DNA. Even though the histone core is overwhelmingly attractive towards the DNA in the radial direction, the histone tails can cause opposing effects, such as H3 and H2A C-terminal.

Correlating our observations on the positions of histone tails with the estimates of electrostatic interactions with DNA, we confirm our hypothesis that they tune DNA unwrapping by the repulsive and attractive forces they exert on DNA, and their inherent conformational variability, in a non-trivial way. This "breaks the symmetry" presented in CG models that only consider the deformation of the DNA and interactions with the histone core, and points to more complex interactions taking place in nucleosomal DNA. We therefore propose the application of our methodology in conjunction with CG models that treat the mechanical properties of the DNA.

CRediT authorship contribution statement

Artemi Bendandi: Conceptualization, Methodology, Formal analysis, Investigation, Writing - original draft, Writing - review & editing, Visualization. **Alessandro S. Patelli:** Formal analysis, Writing - original draft, Visualization. **Alberto Diaspro:** Project administration, Funding acquisition. **Walter Rocchia:** Conceptualization, Methodology, Validation, Writing - review & editing, Supervision.

Declaration of Competing Interest

WR is a co-founder of BiKi Technologies s.r.l., the company that sells the BiKi Life Sciences software suite.

Acknowledgments

ASP was supported by the Swiss National Science Foundation [Grant 200020-182184 to Prof. John H. Maddocks]. WR thanks the ISCRA initiative [project HP10BPTQYQ] for computational hours on GALILEO supercomputer at CINECA.

Appendix A. Supplementary data

Molecular representations of medoids 15, 16, and 17, additional information on the k-medoids clustering analysis, DNA-histone tail proximity plots, and plots of the axial and radial electrostatic forces and the electrostatic potential are provided in the Supplementary Material.

Supplementary data associated with this article can be found, in the online version, at https://doi.org/10.1016/j.csbj.2020.09.034.

References

[1] Biswas M, Voltz K, Smith JC, Langowski J. Role of histone tails in structural stability of the nucleosome. PLoS Comput Biol 2011;7:e1002279.
[2] McGinty RK, Tan S. Nucleosome structure and function. Chem Rev 2014;115:2255–73.

[3] Shaytan AK, Armeev GA, Goncearenco A, Zhurkin VB, Landsman D, Panchenko AR. Coupling between histone conformations and DNA geometry in nucleosomes on a microsecond timescale: Atomistic insights into nucleosome functions. J Mol Biol 2016;428:221–37.
[4] Pasi M, Lavery R. Structure and dynamics of DNA loops on nucleosomes studied with atomistic, microsecond-scale molecular dynamics. Nucleic Acids Res 2016;44:5450–6.
[5] Becker NB, Everaers R. DNA nanomechanics: How proteins deform the double helix. J Chem Phys 2009;130:135102.
[6] Szerlong HJ, Hansen JC. Nucleosome distribution and linker DNA: connecting nuclear function to dynamic chromatin structure. This paper is one of a selection of papers published in a special issue entitled 31st annual international asilomar chromatin and chromosomes conference, and has undergone the journal's usual peer review process. Biochem Cell Biol 2011;89:24–34.
[7] Brandani GB, Niina T, Tan C, Takada S. DNA sliding in nucleosomes via twist defect propagation revealed by molecular simulations. Nucleic Acids Res 2018;46:2788–801.
[8] Freeman GS, Lequieu JP, Hinckley DM, Whitmer JK, de Pablo JJ. DNA shape dominates sequence affinity in nucleosome formation. Phys Rev Lett 2014;113. https://doi.org/10.1103/physrevlett.113.168101.
[9] Rychkov GN, Ilatovskiy AV, Nazarov IB, Shvetsov AV, Lebedev DV, Konev AY, Isaev-Ivanov VV, Onufriev AV. Partially assembled nucleosome structures at atomic detail. Biophys J 2017;112:460–72.
[10] Gansen A, Tóth K, Schwarz N, Langowski J. Opposing roles of h3- and h4-acetylation in the regulation of nucleosome structure–a FRET study. Nucleic Acids Res 2015;43:1433–43.
[11] Kireeva ML, Walter W, Tchernajenko V, Bondarenko V, Kashlev M, Studitsky VM. Nucleosome remodeling induced by RNA polymerase II. Molecular Cell 2002;9:541–52.
[12] Li G, Levitus M, Bustamante C, Widom J. Rapid spontaneous accessibility of nucleosomal DNA. Nature Struct Molecular Biol 2004;12:46–53.
[13] Ozer G, Luque A, Schlick T. The chromatin fiber: multiscale problems and approaches. Current Opinion Struct Biol 2015;31:124–39.
[14] Gebala M, Johnson SL, Narlikar GJ, Herschlag D. Ion counting demonstrates a high electrostatic field generated by the nucleosome. eLife 2019;8. https://doi.org/10.7554/elife.44993.
[15] Rocchia W, Alexov E, Honig B. Extending the applicability of the nonlinear poisson-boltzmann equation: multiple dielectric constants and multivalent ionsy. J Phys Chem B 2001;105:6507–14.
[16] Collepardo-Guevara R, Schlick T. Chromatin fiber polymorphism triggered by variations of DNA linker lengths. Proc National Acad Sci 2014;111:8061–6.
[17] Gan HH, Schlick T. Chromatin ionic atmosphere analyzed by a mesoscale electrostatic approach. Biophys J 2010;99:2587–96.
[18] Izadi S, Anandakrishnan R, Onufriev AV. Implicit solvent model for million-atom atomistic simulations: Insights into the organization of 30-nm chromatin fiber. J Chem Theory Comput 2016;12:5946–59.
[19] Materese CK, Savelyev A, Papoian GA. Counterion atmosphere and hydration patterns near a nucleosome core particle. J Am Chem Soc 2009;131:15005–13.
[20] Baker NA, Sept D, Joseph S, Holst MJ, McCammon JA. Electrostatics of nanosystems: application to microtubules and the ribosome. Proc National Acad Sci 2001;98:10037–41.
[21] Beard DA, Schlick T. Modeling salt-mediated electrostatics of macromolecules: The discrete surface charge optimization algorithm and its application to the nucleosome. Biopolymers 2001;58:106–15.
[22] Kato H, Gruschus J, Ghirlando R, Tjandra N, Bai Y. Characterization of the n-terminal tail domain of histone h3 in condensed nucleosome arrays by hydrogen exchange and NMR. J Am Chem Soc 2009;131:15104–5.
[23] Saurabh S, Glaser MA, Lansac Y, Maiti PK. Atomistic simulation of stacked nucleosome core particles: Tail bridging, the h4 tail, and effect of hydrophobic forces. J Phys Chem B 2016;120:3048–60.
[24] Widom J. Chromatin: The nucleosome unwrapped. Current Biol 1997;7: R653–5.
[25] Andresen K, Jimenez-Useche I, Howell SC, Yuan C, Qiu X. Solution scattering and FRET studies on nucleosomes reveal DNA unwrapping effects of h3 and h4 tail removal. PLoS ONE 2013;8:e78587.
[26] Bertin A, Leforestier A, Durand D, Livolant F. Role of histone tails in the conformation and interactions of nucleosome core particlesy. Biochemistry 2004;43:4773–80.
[27] Winogradoff D, Echeverria I, Potoyan DA, Papoian GA. The acetylation landscape of the h4 histone tail: Disentangling the interplay between the specific and cumulative effects. J Am Chem Soc 2015;137:6245–53.
[28] Zhou B-R, Feng H, Ghirlando R, Kato H, Gruschus J, Bai Y. Histone h4 k16q mutation, an acetylation mimic, causes structural disorder of its n-terminal basic patch in the nucleosome. J Mol Biol 2012;421:30–7.
[29] Gao M, Nadaud PS, Bernier MW, North JA, Hammel PC, Poirier MG, Jaroniec CP. Histone h3 and h4 n-terminal tails in nucleosome arrays at cellular concentrations probed by magic angle spinning NMR spectroscopy. J Am Chem Soc 2013;135:15278–81.
[30] Mauney AW, Tokuda JM, Gloss LM, Gonzalez O, Pollack L. Local DNA sequence controls asymmetry of DNA unwrapping from nucleosome core particles. Biophys J 2018;115:773–81.
[31] Norouzi D, Zhurkin VB. Dynamics of chromatin fibers: comparison of monte carlo simulations with force spectroscopy. Biophys J 2018;115:1644–55.
[32] Fan Y, Korolev N, Lyubartsev AP, Nordenskiöld L. An advanced coarse-grained nucleosome core particle model for computer simulations of nucleosome-nucleosome interactions under varying ionic conditions. PLoS ONE 2013;8: e54228.
[33] Becker NB, Everaers R. DNA nanomechanics in the nucleosome. Structure 2009;17:579–89.
[34] Shaytan AK, Armeev GA, Goncearenco A, Zhurkin VB, Landsman D, Panchenko AR. Trajectories of microsecond molecular dynamics simulations of nucleosomes and nucleosome core particles. Data Brief 2016;7:1678–81.
[35] Davey CA, Sargent DF, Luger K, Maeder AW, Richmond TJ. Solvent mediated interactions in the structure of the nucleosome core particle at 1.9Å resolution. J Mol Biol 2002;319:1097–113.
[36] Decherchi S, Spitaleri A, Stone J, Rocchia W. NanoShaper–VMD interface: computing and visualizing surfaces, pockets and channels in molecular systems. Bioinformatics 2018;35:1241–3.
[37] Dolinsky TJ, Nielsen JE, McCammon JA, Baker NA. PDB2pqr: an automated pipeline for the setup of poisson-boltzmann electrostatics calculations. Nucleic Acids Res 2004;32:W665–7.
[38] Decherchi S, Rocchia W. A general and robust ray-casting-based algorithm for triangulating surfaces at the nanoscale. PLoS ONE 2013;8:e59744.
[39] Cock PJA, Antao T, Chang JT, Chapman BA, Cox CJ, Dalke A, Friedberg I, Hamelryck T, Kauff F, Wilczynski B, de Hoon MJL. Biopython: freely available python tools for computational molecular biology and bioinformatics. Bioinformatics 2009;25:1422–3.
[40] Edayathumangalam RS, Weyermann P, Dervan PB, Gottesfeld JM, Luger K. Nucleosomes in solution exist as a mixture of twist-defect states. J Mol Biol 2005;345:103–14.
[41] Tachiwana H, Kagawa W, Osakabe A, Kawaguchi K, Shiga T, Hayashi-Takanaka Y, Kimura H, Kurumizaka H. Structural basis of instability of the nucleosome containing a testis-specific histone variant, human h3t. Proc National Acad Sci 2010;107:10454–9.
[42] Jin J, Bai L, Johnson DS, Fulbright RM, Kireeva ML, Kashlev M, Wang MD. Synergistic action of RNA polymerases in overcoming the nucleosomal barrier. Nature Struct Mol Biol 2010;17:745–52.
[43] Iwasaki W, Miya Y, Horikoshi N, Osakabe A, Taguchi H, Tachiwana H, Shibata T, Kagawa W, Kurumizaka H. Contribution of histone nterminal tails to the structure and stability of nucleosomes. FEBS Open Bio 2013;3:363–9.
[44] Kono H, Sakuraba S, Ishida H. Free energy profiles for unwrapping the outer superhelical turn of nucleosomal DNA. PLOS Comput Biol 2018;14:e1006024.
[45] Brower-Toland B, Wacker DA, Fulbright RM, Lis JT, Kraus WL, Wang MD. Specific contributions of histone tails and their acetylation to the mechanical stability of nucleosomes. J Mol Biol 2005;346:135–46.
[46] Tims HS, Gurunathan K, Levitus M, Widom J. Dynamics of nucleosome invasion by DNA binding proteins. J Mol Biol 2011;411:430–48.
[47] Ferreira H, Somers J, Webster R, Flaus A, Owen-Hughes T. Histone tails and the h3 n helix regulate nucleosome mobility and stability. Mol Cellular Biol 2007;27:4037–48.
[48] Kim J-A, Hsu J-Y, Smith MM, Allis CD. Mutagenesis of pairwise combinations of histone amino-terminal tails reveals functional redundancy in budding yeast. Proc National Acad Sci 2012;109:5779–84.
[49] Kameda T, Awazu A, Togashi Y. Histone tail dynamics in partially disassembled nucleosomes during chromatin remodeling. Front Mol Biosci 2019;6. https://doi.org/10.3389/fmolb.2019.00133.
[50] Kulaeva OI, Zheng G, Polikanov YS, Colasanti AV, Clauvelin N, Mukhopadhyay S, et al. Internucleosomal interactions mediated by histone tails allow distant communication in chromatin. J Biolog Chem 2012;287:20248–57.
[51] Potoyan DA, Papoian GA. Regulation of the h4 tail binding and folding landscapes via lys-16 acetylation. Proc Nat Acad Sci 2012;109:17857–62.
[52] Wang X, Moore SC, Laszckzak M, Ausió J. Acetylation increases the a-helical content of the histone tails of the nucleosome. J Biolog Chem 2000;275:35013–20.
[53] Anderson J, Lowary P, Widom J. Effects of histone acetylation on the equilibrium accessibility of nucleosomal DNA target sites 1 1edited by r. ebright. J Mol Biol 2001;307:977–85.
[54] Polach K, Lowary P, Widom J. Effects of core histone tail domains on the equilibrium constants for dynamic dna site accessibility in nucleosomes. J Mol Biol 2000;298:211–23.
[55] Patelli AS, A sequence-dependent coarse-grain model of b-dna with explicit description of bases and phosphate groups parametrised from large scale molecular dynamics simulations, 261 (2019)..